Mechatronics 110 (2025) 103354

Contents lists available at ScienceDirect

Mechatronics

journal homepage: www.elsevier.com/locate/mechatronics

Modeling and feedforward control of hysteresis in piezoelectric actuators considering its rotation and expansion☆

Yunzhi Zhang [a], Jie Ling [a,*], Micky Rakotondrabe [b], Yuchuan Zhu [a], Dan Wang [a]

[a] College of Mechanical and Electrical Engineering, Nanjing University of Aeronautics and Astronautics, Nanjing 210016, Jiangsu, China
[b] Laboratoire Génie de Production, University of Technologie Tarbes Occitanie Pyrénées (UTTOP), University of Toulouse alliance, Tarbes 65016, France

ARTICLE INFO

Keywords:
Rate-dependent hysteresis
Piezoelectric actuators
Feedforward control
Hammerstein architecture

ABSTRACT

Piezoelectric actuators (PEAs) play a key role in precision engineering, but their strong rate-dependent hysteresis affects accuracy. Existing hysteresis models fail to capture the simultaneous rotation and expansion of hysteresis at high rates. This paper proposes a modified Prandtl–Ishlinskii model in a Hammerstein-like architecture (HAMPI) aiming to model the rotation and expansion of the hysteresis at different input rates. Simulations and experiments are conducted to validate the HAMPI model across a wide range of input rates (50–500 Hz) and amplitudes (0–140 V), revealing that the proposed model has the root-mean-square error (resp. relative root-mean-square error) of 0.47 μm (resp. 3.07%), which is lower than the results of existing hysteresis model. Additionally, a HAMPI-based feedforward controller with the inverse multiplicative structure shows that the tracking performance RMS error (resp. NRMS error) can be kept within 0.09 μm (resp. 2.25%) when the operating frequency is below 150 Hz. Meanwhile, the displacement attenuation issue in feedforward control caused by the rate-dependent rotation of hysteresis loops is also successfully addressed by the proposed HAMPI model.

1. Introduction

Owing to high precision, high resolutions, fast response, and compact structure, piezoelectric actuators (PEA) are widely used in nanopositioning instruments, aeronautical actuation systems, and other applications requiring quick response and precision motion [1–3].

However, the inherent strong rate-dependent asymmetric hysteresis gives rise to the inaccuracy in open-loop control and causes undesirable oscillations in the closed loop [4]. The specific performance of the dynamic hysteresis is as follows: with the increase of rate, a clockwise rotation of the hysteresis loop and an expansion in width will occur, as shown in Fig. 1. The data in this figure comes from the author's laboratory, while similar results can be found in [5,6].

Many studies aim to reduce the impact of rate-dependent hysteresis on the accuracy of PEAs. These methods are divided into two categories: (i) feedback control without hysteresis models and (ii) feedforward control with hysteresis models [4,7]. Feedback control uses nonlinear techniques (e.g., repetitive, iterative learning, sliding mode, and fuzzy control) to handle hysteresis as disturbances [8–10]. Feedback control gives robustness against uncertainties and disturbances, but it faces some limitations in practical use. Firstly, feedback for compact systems like micro/nano actuators is strongly limited by the difficulty of integrating the sensor [11]. Secondly, the control gain will be limited for the stability of the closed-loop system, so feedback control is relatively difficult to use in high-speed position tracking [12].

In contrast, feedforward control designed by leveraging prior knowledge does not require sensor integration. At the same time, combining feedback and feedforward control can significantly enhance the bandwidth of the closed-loop system, improving the high-speed positioning accuracy of the piezoelectric actuator [13]. Hence, designing an effective feedforward controller is a great need for hysteresis compensation and PEA's high-speed position tracking. The designing process of a feedforward controller for PEAs involves: (1) developing an accurate hysteresis model that captures the dynamic behavior of PEAs, and (2) applying either the inverse or direct form of the hysteresis model as the feedforward controller [11].

☆ This paper was recommended for publication by Associate Editor Oliver Sawodny.

* Corresponding author.
E-mail addresses: jxzyz@nuaa.edu.cn (Y. Zhang), meejling@nuaa.edu.cn (J. Ling), mrakoton@uttop.fr (M. Rakotondrabe), meeyczhu@nuaa.edu.cn (Y. Zhu), wangdan_053@nuaa.edu.cn (D. Wang).

https://doi.org/10.1016/j.mechatronics.2025.103354
Received 30 December 2024; Received in revised form 25 April 2025; Accepted 16 May 2025
Available online 4 June 2025

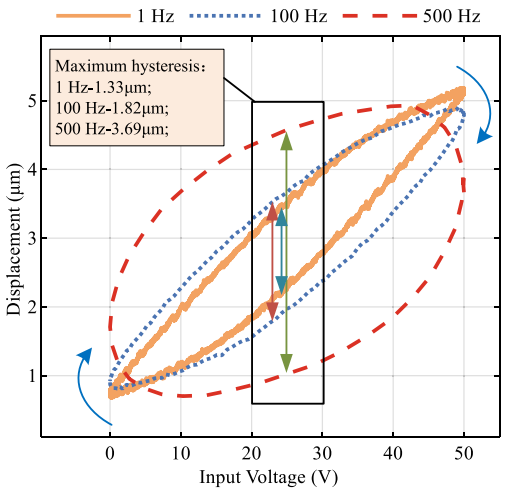

Fig. 1. Rotation and expansion of the hysteresis loop with increasing rates (data measured from the author's laboratory).

Two primary methods are commonly used to construct a rate-dependent hysteresis model. The first approach incorporates dynamic factors into a static hysteresis model, making it rate-dependent. Thanks to the flexibility of modeling and modification, lots of studies have been done on operator-based hysteresis models, like the Preisach model [14] and Prandtl–Ishlinskii (PI) model. Modified dynamic operators are developed by combining the derivative of the input signal with parameters or functions including thresholds [15,16], envelope functions [17] or weights [5] of the operators. However, these methods still have limitations in modeling the expanding and rotating hysteresis loops. Firstly, considering that positive excitation is utilized to drive PEAs in practice, the approach of dynamic thresholds will lose its accuracy at the descending branch of the hysteresis loops when a one-side play operator is used [18]. About this aspect, building rate-dependent envelope functions or dynamic weights is more accurate and suitable, but it is difficult to design suitable envelope functions or weights considering the expansion and rotation simultaneously.

The second approach employs the Hammerstein architecture, which includes a static hysteresis model cascaded with a linear dynamic model. Hammerstein architecture with classical PI model [19], Bouc–Wen (BW) model [20] and Preisach model [21] are studied. While effective for describing hysteresis loop expansion, these models struggle to capture the dynamic rotation of hysteresis loops at high rates accurately. Since the Hammerstein architecture is well-suited for describing expansion, incorporating dynamic factors in the Hammerstein model allows for the rotation modeling on top of the expanding loop. Some works have been done to revise the Hammerstein architecture to a Hammerstein-like architecture in which hysteresis models are rate-dependent. The modified PI model with dynamic weights is introduced to the Hammerstein-like architecture in [22], but the frequency range for model validation is limited to 60 Hz, and the model accuracy is already insufficient at 60 Hz. A Hammerstein-like architecture with a modified PI model revised by dynamic envelop functions is studied in [17], this model improves the accuracy in 1–50 Hz compared to other hysteresis models. Hence, models developed in the above work show the potential of Hammerstein-like architecture with rate-dependent hysteresis models in accounting for the rotation and expansion of hysteresis loops. However, the existing models have not been validated in the high-frequency range (> 200 Hz), whereas in the low-frequency range (< 100 Hz), the hysteresis rotational characteristics are not significant.

This paper introduces a novel modified PI model with a Hammerstein-like architecture (HAMPI) that simultaneously captures two dynamic hysteresis phenomena at high frequencies (50–500 Hz). The key contribution of this work lies in the innovative modified PI model, which incorporates a new formulation of dynamic weights specifically designed to address the two dynamic hysteresis behaviors. Additionally, the paper presents a comprehensive method for parameter identification and develops a complete open-loop feedforward controller based on the HAMPI model. Extensive validation is carried out across a wide range of input frequencies (50–500 Hz) and amplitudes (0–140 V), highlighting the model's effectiveness. Furthermore, experiments with the feedforward controller provide additional evidence of the proposed model's superiority.

The remainder of this paper is organized as follows. Section 2 makes the evaluation of Hammerstein architecture in modeling rate-dependent hysteresis. In Section 3, the modified PI model with Hammerstein-like architecture (HAMPI) is developed, including a detailed design process, followed by its parameter identification. Section 4 presents the development of the feedforward controller based on the HAMPI model. Section 5 presents simulation and experimental evaluations of the proposed model and the feedforward controller based on it. The model comparison is carried out between the rate-dependent PI (RDPI) model, the classical PI model with Hammerstein architecture (HAPI), and the proposed HAMPI model. Additionally, a comparison of control effects is performed between the feedforward controller based on the HAPI model and the HAMPI model for further evaluation. Finally, Section 6 offers the conclusions.

2. Evaluation of hammerstein architecture in modeling rate-dependent hysteresis

Expansion and rotation are two rate-dependent hysteresis phenomena of PEAs observed from the hysteresis loops, as Fig. 1 shows. To model these rate-dependent hysteresis effects, the Hammerstein architecture is employed, where the linear dynamics model within the architecture plays a crucial role in capturing both the expansion and rotation behaviors. This section aims to assess whether the identified linear dynamics model accurately represents these two phenomena and evaluates the effectiveness of the Hammerstein architecture in modeling rate-dependent hysteresis.

To begin, a low-amplitude (10 V) step response is applied to the piezoelectric actuator in order to minimize the influence of hysteresis on the identification results of the linear dynamics model. The step response identification method contains system information across the entire frequency range, and thus it is commonly used as a method for identifying the linear dynamics of piezoelectric systems. The linear time-invariant (LTI) dynamics model is then derived using the Identification Toolbox of MATLAB. The resulting model can be expressed as

$$G(s) = \frac{-340.5s^2 + 4.249 \times 10^6 s + 3.461 \times 10^7}{s^3 + 8610s^2 + 5.989 \times 10^7 s + 4.751 \times 10^8} \tag{1}$$

where the fitness between the measured data and the identified model is 93.56%, as shown in Fig. 2. Fig. 3 shows the bode diagram of the identified linear dynamics model of the PEA. It can be found in the frequency range of 1–500 Hz, the system's amplitude–frequency curve first decreases and then increases, while the phase–frequency curve of the system continues to decrease.

Furthermore, through driving the PEA with harmonic signals at different frequencies (1–500 Hz) and 0–50 V, the system's time-domain response can be found in Fig. 4. To analyze the relationship between the input signal and output displacement of PEA, Fig. 4(a) takes the number of samples as the X-axis, while the Y-axis is the displacement ratio which means the values of the reference and the output are scaled proportionally. The input signal is added to Fig. 4(a) as the reference. Fig. 4(b) is the corresponding hysteresis loop. It can be observed from Fig. 4 that the phase lag is the main reason for the expansion and rotation.

From Figs. 3 and 4, it can be observed that the dynamic characteristics of the identified model are generally consistent with the

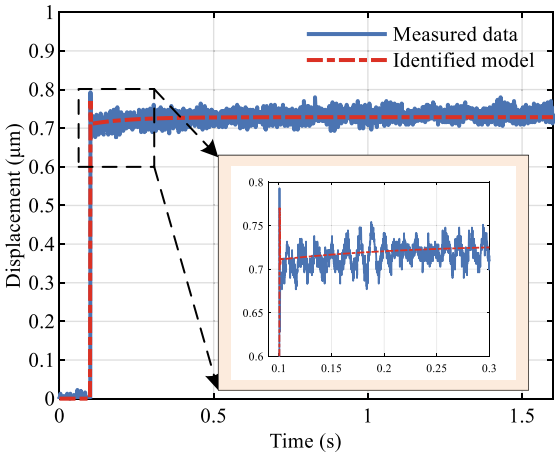

Fig. 2. Comparison of the measured data and the identified linear dynamics model under step response test.

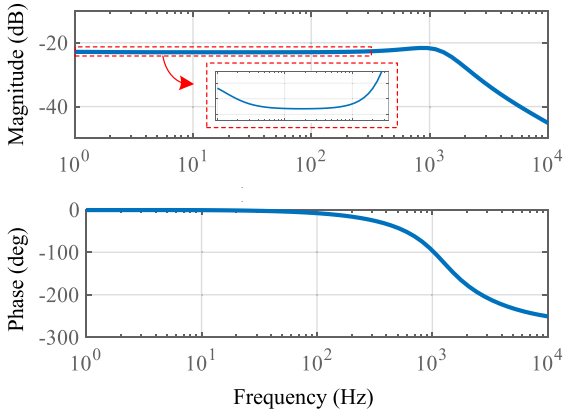

Fig. 3. Bode diagram of the identified linear dynamics model.

Table 1
The phase lag of the LTI model and the experimental data with harmonic signals.

Frequency (Hz)	LTI model (deg)	Experimental data (deg)
1	0	0
50	2.8	2.25
100	6.3	7.65
300	21.3	27.5
500	39.0	49.1

experimental data under harmonic signals driving. However, as Table 1 shows, through a quantitative analysis of the phase lag of the identified linear dynamics model at each frequency, it can be found that there is some error compared to the experimental results with harmonic signals (phase lag caused by hysteresis has been removed). Meanwhile, the error is enlarged with the rise in frequency. Hence, the identified linear dynamics model fails to accurately express the rotation caused by the phase lag.

In practice, due to the limitations of the hardware sampling rate and the accuracy of the sensing equipment, high-frequency information under small amplitude step driving tends to be mixed with high-frequency noise from the sensors, while it is also difficult to ensure sufficient high-frequency information is captured. Hence, the identified linear dynamics model cannot accurately describe the phase lag, which is the reason why the Hammerstein architecture fails to model the rotation and expansion of hysteresis loops simultaneously.

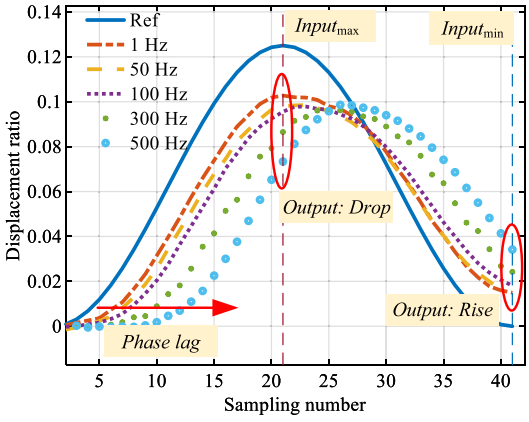

(a) Displacement ratio of the first period

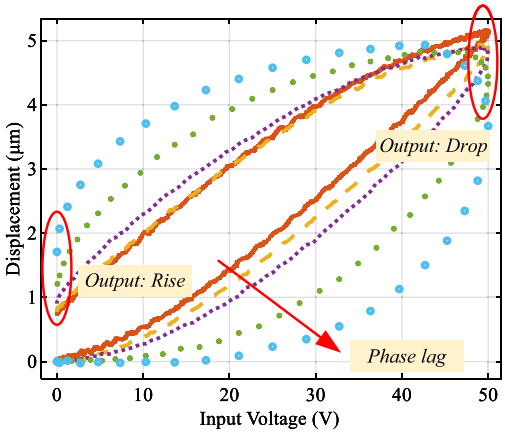

(b) Hysteresis loop of the first period

Fig. 4. Comparison of the displacement and phase lag between different rates in the first period.

3. Rate-dependent hysteresis modeling

3.1. Modified Prandtl–Ishlinskii model

This paper proposes a modified Prandtl–Ishlinskii model with the Hammerstein-like architecture. Different from the existing Hammerstein architecture with a classical PI model, the modified PI model incorporates a new formulation of dynamic weights designed directly based on the rotation and expansion of hysteresis loops.

The classical PI model integrates a series of backlash operators $H_{r_i}(\cdot)$ with different thresholds r_i and different weights w_i to describe the hysteresis nonlinear phenomenon of PEAs. When an input $u(\cdot) \in C[0,T]$, which means $u(\cdot)$ is a continuous function on the time interval $[0,T]$, is applied to PEAs, the output of the PI model is given by the formula as

$$Y[u](t) = w_0 u(t) + \sum_{i=1}^{n} w_i H r_i[u](t), \quad i = 1, 2, \ldots, n \tag{2}$$

where n represents the number of backlash operators, w_i means the weights of each operator, and r_i are positive thresholds [23].

Backlash operators $H_{r_i}(\cdot)$ can be described in the following formula as

$$H r_i[u](t) = max\left\{u(t) - r_i, min(u(t) + r_i, H r_i[u](t - t_s))\right\} \tag{3}$$

where t_s means the sampling period.

The modified PI model uses dynamic weights, including static weights $w_i(\cdot)$, rotation weights $w_r(\cdot)$, and adaptive weights $w_a(\cdot)$. Static

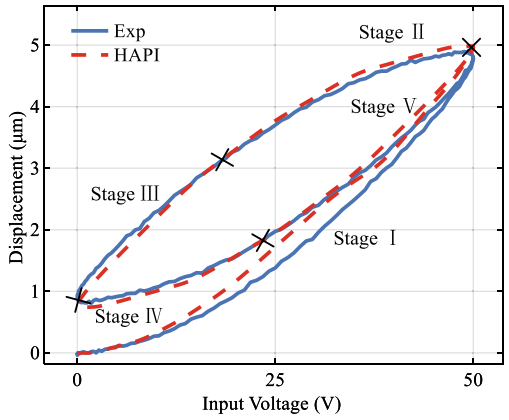

Fig. 5. Stage division for weights' changing according to the comparison between experimental data and HAPI model.

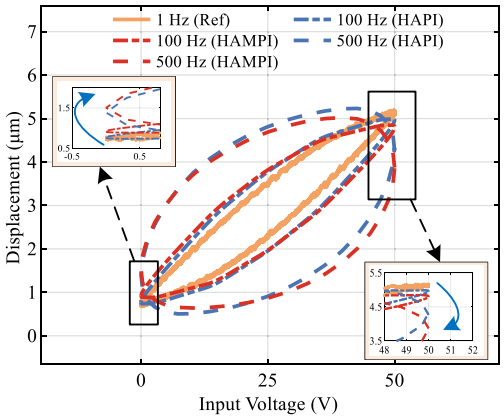

Fig. 6. Comparison of HAPI model and HAMPI model in different rates.

weights describe hysteresis under (quasi-) static conditions, while rotation and adaptive weights convert static weights into dynamic ones, capturing rotation effects. The novel dynamic weights $wd_i(\cdot)$ can be designed as

$$wd_i(w_i, u, \dot{u}) = w_i + w_r(\dot{u}) + w_a(u) \tag{4}$$

$$\begin{cases} w_r(\dot{u}) = [-\varepsilon(\dot{u})m_1 + \varepsilon(-\dot{u})m_2]\dot{u} \\ w_a(u) = ku + b \\ \varepsilon(\dot{u}) = \begin{cases} 1, & \dot{u}(t) \geq 0 \\ 0, & \dot{u}(t) < 0 \end{cases} \end{cases} \tag{5}$$

where m_1 and m_2 are two positive constants, $\varepsilon(\cdot)$ is a logic function compared to zero. k and b are constants and k is negative and b is positive. The rotation operator $w_r(\cdot)$ is designed with the derivative of the input signal.

Then, the modified PI model can be obtained as

$$Y[u](t) = \sum_{i=1}^{n} wd_i H r_i[u](t) \tag{6}$$

where $Y[u](\cdot)$ is the output of the model.

Principle of the novel dynamic weights: The proposed modified PI model explains the rotation of hysteresis loops in five stages, as shown in Fig. 5. These stages compare the hysteresis loop of Hammerstein architecture with the classical PI model (HAPI) with experimental data, highlighting differences and corrections by the modified PI model. If the HAPI model's curve is lower than the experimental data, the weights of the operators need to be increased to get close to the experimental loop, and vice versa. This principle shows that the positive constants m_1 and m_2 make $w_r(\cdot)$ negative in stages I, II, and V. To correct stages III and IV, $w_a(\cdot)$, a positive linear function of the input signal $u(\cdot)$ compensates for errors, adjusting weights at the start and end of each period. Here, the constant k needs to be set to a negative value, while the constant b is positive. This is because it has been observed that as the input voltage increases, the difference between the HAPI model's curve and the HAMPI model's curve gradually decreases.

Integrating the modified PI model with the Hammerstein-like architecture (HAMPI), the overall model designed in this paper to account for the rotation and expansion of hysteresis loops is gained. The comparison of the HAPI model and the HAMPI model is shown in Fig. 6. It can be observed that the HAMPI model has the ability to describe the rotation phenomenon of the hysteresis loop at a wide range of rates.

3.2. Parameter identification of the HAMPI model

Since the HAMPI model consists of the modified PI model and linear dynamics part. The parameter identification can be divided into three parts. Firstly, the parameters of the linear dynamics are identified through the open-loop test of step response, the initial value is 0 V while the final value is 10 V. The linear dynamics model from the input voltage to the output displacement of the PEA is obtained as Eq. (1) shows.

Table 2
The parameters of the static hysteresis part.

Number	r_i	w_i	Number	r_i	w_i
1	0.5	0.58	6	28.5	−0.37
2	5.5	0.47	7	35	0.66
3	10.5	0.26	8	41.5	−0.14
4	15.5	0.28	9	45	0.18
5	22	−0.04	10	49	−0.50

Based on the identified linear dynamics model, the second step is to identify the modified PI model's static weights w_i through a quasi-static open-loop test, while the rotation weights $w_r(\cdot)$ and adaptive weights $w_a(\cdot)$ are set as zero. The input signal is sinusoidal signals of 1 Hz and 0–50 V. Here the threshold value r_i is chosen as Table 2 shows.

The parameter identification is conducted in MATLAB and the cost function is set to minimize the sum squared error. The optimization method is Nonlinear least squares and the algorithm is Trust-Region-Reflective. It should be mentioned that w_i is identified based on linear dynamics. The parameters of the static hysteresis part are listed in Table 2.

The third step is to identify the parameters of the modified PI model for dynamic modification, including m_1, m_2, k, and b. Since the modeling error of Hammerstein architecture with classical PI model mainly occurs above 100 Hz, the PEAs' response of the sinusoidal signal of 100 Hz and 50 V is chosen to identify the parameters for dynamic modification. Through the parameter identification at this single frequency, the goal is to obtain parameters that can describe the hysteresis at frequencies above 100 Hz. The method of identification is the same as the second step. The parameters of this part are: $m_1 = 7.7 \times 10^{-7}$, $m_2 = 2.5 \times 10^{-7}$, $k = -6.4 \times 10^{-4}$ and $b = 0.025$. Fig. 7 shows the steps and flow of the parameter identification.

4. Feedforward controller design with HAMPI model

This paper designs a feedforward controller for complete open-loop control. The model of PEA is divided into two parts according to the HAMPI model. One part is the modified PI model, the other is the linear dynamics. The compensators are designed individually for the two parts to compensate for the rate-dependent hysteresis. In this section, an approximate inverse of linear dynamics is calculated to compensate for the linear dynamics. The inverse multiplicative structure with the modified PI model is designed to compensate for the modified PI model.

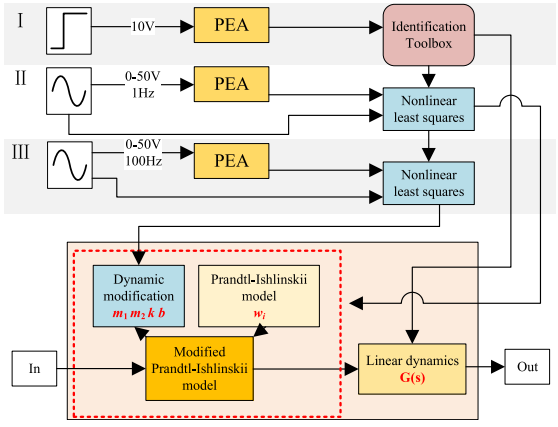

Fig. 7. The flow chart of the parameter identification.

4.1. Approximate inverse of linear dynamics

According to the linear dynamics identified by the step response, it can be found that the order of the denominator term of the transfer function is greater than that of the numerator term. Furthermore, as Eq. (7) shows, it is a non-minimum phase system containing a positive zero.

$$G(s) = \frac{-340.48(s - 1.249 \times 10^4)(s + 8.14)}{(s + 7.942)(s^2 + 8602s + 5.982 \times 10^7)} \tag{7}$$

Hence, direct inversion of the dynamic part will result in non-causal feedforward input. Three kinds of approximate inverse methods are used to compensate for the dynamics, according to the following algorithm under the discrete time domain

$$\hat{G}^{-1}(z) = \frac{z^{-q} A(z) B_u^*(z)}{B_s(z)} \tag{8}$$

Here, z^{-q} is the delay term, $A(z)$ is the denominator of the discrete transfer function respectively, $B_s(z)$ is the numerator of the minimum phase system, $B_u^*(z)$ is the stable approximate inverse of the $B_u(z)$, which is the numerator of the non-minimum phase system.

According to the identified model as Eq. (7) shows, the model under the discrete time domain can be gained by the Tustin method, the sampling time is 0.1 ms.

$$G(z) = -0.0047 \frac{(z + 1)(z - 1.908)}{z^2 - 1.537z + 0.6566} \tag{9}$$

Hence, the numerator of the non-minimum phase system $B_u(z)$ is

$$B_u(z) = z - 1.908 \tag{10}$$

Table 3 is the calculation of the three kinds of approximate inverse methods of $B_u(z)$, including Zero-phase-error tracking control (ZPETC), Zero-magnitude-error tracking control (ZMETC) and Nonminimum-phase zeros ignore (NPZ-Ignore). Fig. 8 shows their compensating results. It can be found that ZPETC is the best one considering the magnitude and phase lag between 10–500 Hz, which is the working condition of the PEA.

Hence, the approximate inverse based on ZPETC is calculated as

$$\hat{G}^{-1}(z) = \frac{1.908z^4 - 2.025z^3 - 1.143z^2 + 2.133z - 0.657}{0.015z^4} \tag{11}$$

Since the linear dynamics and modified PI model are continuous time-domain. Hence, transfer the approximate inverse in Eq. (11), to the approximate inverse in continuous time-domain with the Tustin method. The approximate inverse can be calculated as

$$\hat{G}^{-1}(s) = \frac{\begin{array}{l}2.594 \times 10^{-2} s^4 + 4.818 \times 10^7 s^3 + \\ 1.016 \times 10^{12} s^2 + 8.062 \times 10^{15} s + 3.593 \times 10^{19}\end{array}}{\begin{array}{l}s^4 + 1.6 \times 10^5 s^3 + 9.6 \times 10^9 s^2 \\ +2.56 \times 10^{14} s + 2.56 \times 10^{18}\end{array}} \tag{12}$$

Table 3
Calculation of approximate inverse method [24,25].

Approximate inverse method	$B_u^*(z)$
ZPETC	$\frac{1}{B_u(1)}$
ZMETC	$\frac{B_u(z^{-1})}{[B_u(1)]^2}$
NPZ-Ignore	$\frac{1}{B_u(z^{-1})}$

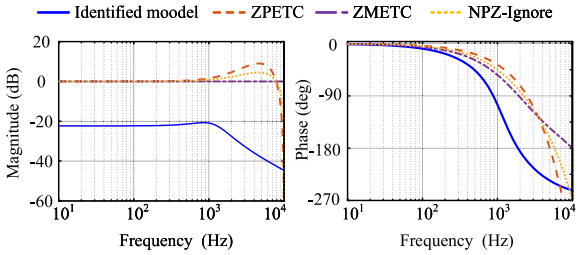

Fig. 8. Bode diagram of the identified model compensated by the three kinds of approximate inverse.

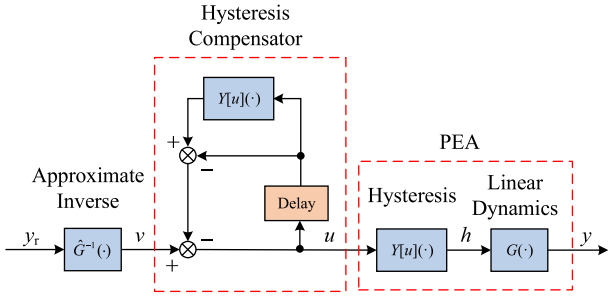

Fig. 9. Block diagram of the feedforward control of the PEA.

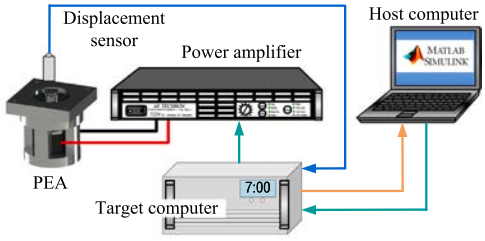

(a) Test signal flow

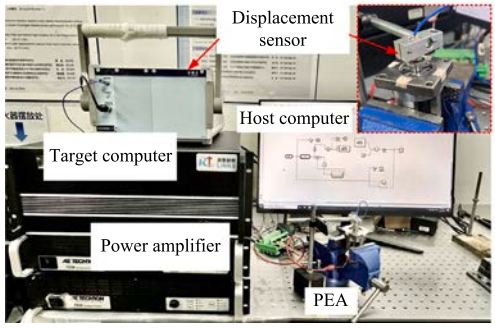

(b) Test platform

Fig. 10. Experimental platform for the test of the PEA.

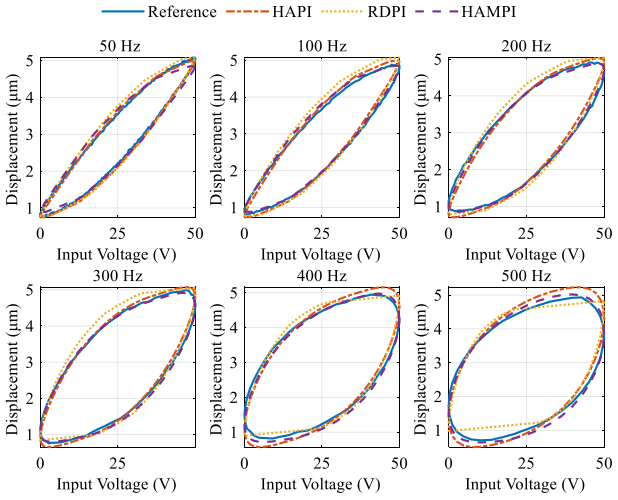

Fig. 11. Comparison and verification of HAPI, RDPI and HAMPI model in different input rates and amplitude of 50 V.

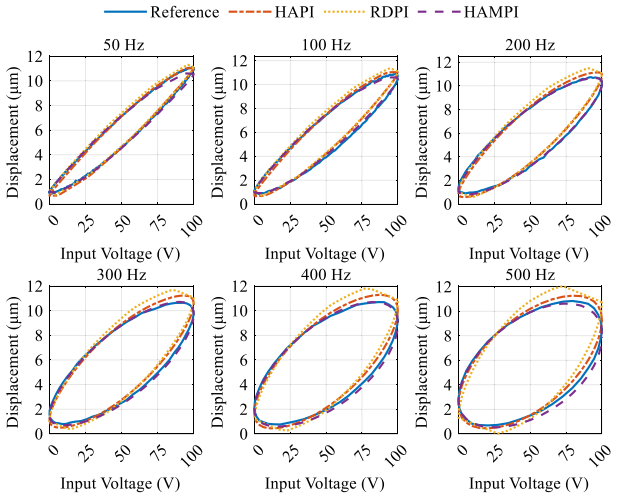

Fig. 12. Comparison and verification of HAPI, RDPI and HAMPI model in different input rates and amplitude of 100 V.

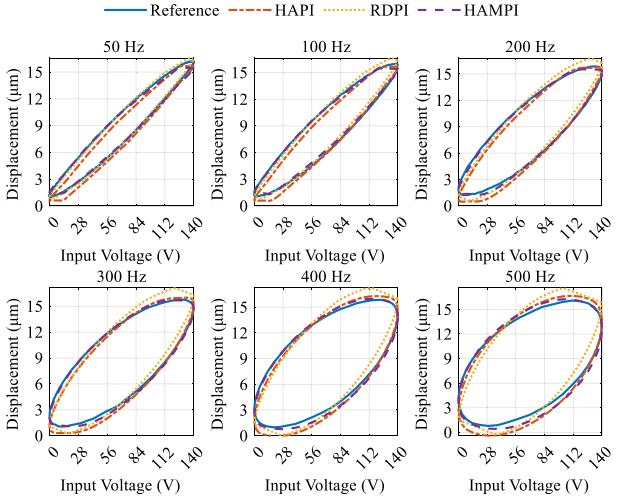

Fig. 13. Comparison and verification of HAPI, RDPI and HAMPI model in different input rates and amplitude of 140 V.

4.2. Inverse multiplicative structure with HAMPI

Since the modified Prandtl–Ishlinskii model contains the logic function and derivative of input signal, which brings difficulty in calculating its inversion. The inverse multiplicative structure with hysteresis model is an inversion-free method to compensate for the hysteresis part [26]. As soon as the model is identified, the compensator is directly derived without additional calculation. As shown in Fig. 9, the feedforward controller with the inverse multiplicative structure and modified Prandtl–Ishlinskii model is designed for hysteresis cancellation.

Theorem 1. *For a PEA system in Eq. (6), if the control law is:*

$$u(t) = v(t) + u(t - t_s) - Y[u](t - t_s) \tag{13}$$

and the sampling time t_s is small enough, the compensation for the PEA's hysteresis nonlinearity can be achieved, as Eq. (14) shows:

$$\frac{\mathrm{d}h}{\mathrm{d}v} \approx 1 \tag{14}$$

Proof. As Fig. 9 shows, the hysteresis can be written as follows:

$$h(t) = Y[u](t) = -u(t) + u(t) + Y[u](t) \tag{15}$$

Assume the relationship between $v(t)$ and $h(t)$ is:

$$h(t) = v(t) + O(t) \tag{16}$$

and $O(t)$ is obtained by Eqs. (13) and (15) as:

$$O(t) = u(t - t_s) - u(t) + Y[u](t) - Y[u](t - t_s) \tag{17}$$

Calculate the derivative of the output $h(t)$ with respect to the control signal $v(t)$ by Eq. (16):

$$\frac{\mathrm{d}h}{\mathrm{d}v} = 1 + \frac{\partial O}{\partial v} \tag{18}$$

From Eq. (17), we have:

$$\begin{aligned} \frac{\mathrm{d}O(t)}{\mathrm{d}v(t)} &= \frac{\mathrm{d}u(t-t_s)-u(t)}{\mathrm{d}v(t)} + \frac{\mathrm{d}(Y[u](t)-Y[u](t-t_s))}{\mathrm{d}v(t)} \\ &= \left[\frac{\partial u(t-t_s)}{\partial v(t)} - \frac{\partial u(t)}{\partial v(t)}\right] + \left[\frac{\partial Y[u](t)}{\partial v(t)} - \frac{\partial Y[u](t-t_s)}{\partial v(t)}\right] \end{aligned} \tag{19}$$

Here, $\frac{\partial Y[u](t-t_s)}{\partial v(t)}$ can be expanded using Taylor series as:

$$\frac{\partial Y[u]\left(t - t_s\right)}{\partial v(t)} \approx \frac{\partial Y[u](t)}{\partial v(t)} - t_s \cdot \frac{\partial}{\partial t}\left(\frac{\partial Y[u](t)}{\partial v(t)}\right) \tag{20}$$

Hence, Eq. (21) can be obtained if the sampling time t_s is small enough:

$$\frac{\partial Y[u](t)}{\partial v(t)} - \frac{\partial Y[u](t - t_s)}{\partial v(t)} \approx 0 \tag{21}$$

A similar conclusion can be deduced based on the method above that:

$$\frac{\partial u\left(t - t_s\right)}{\partial v(t)} \approx \frac{\partial u(t)}{\partial v(t)} - t_s \cdot \frac{\partial}{\partial t}\left(\frac{\partial u(t)}{\partial v(t)}\right) \tag{22}$$

$$\frac{\partial u(t)}{\partial v(t)} - \frac{\partial u(t - t_s)}{\partial v(t)} \approx 0 \tag{23}$$

Hence, Eq. (24) can be obtained by Eqs. (18)–(23):

$$\frac{\mathrm{d}h}{\mathrm{d}v} = 1 + \frac{\partial O}{\partial v} \approx 1 \tag{24}$$

Here, $u(\cdot)$ is the control force applied to PEAs, $h(\cdot)$ is the hysteresis of PEAs, $Y[u](\cdot)$ is the output of the HAMPI model, $v(\cdot)$ is an intermediate variable calculated from the approximate inversion $\hat{G}^{-1}(\cdot)$. Theorem 1 is proved and the effect of the compensator depends on the sampling time t_s according to Eqs. (20) and (22).

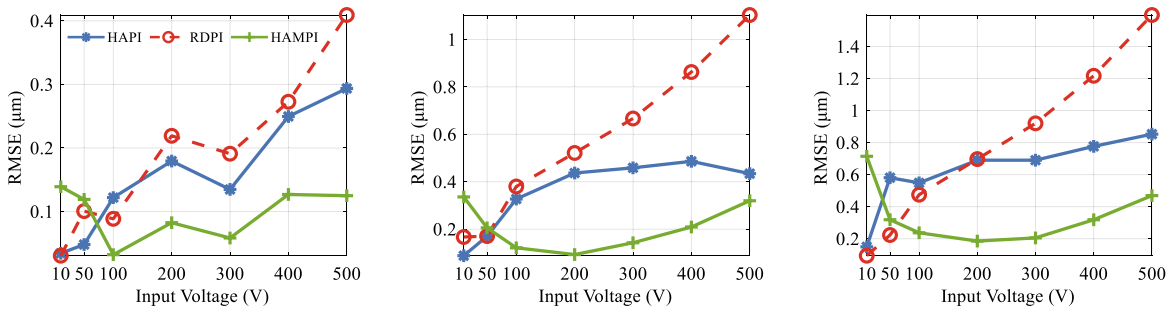

(a) RMSE of HAPI, RDPI and HAMPI model under 50 V (b) RMSE of HAPI, RDPI and HAMPI model under 100 V (c) RMSE of HAPI, RDPI and HAMPI model under 140 V

Fig. 14. Accuracy verification of the HAMPI model in hysteresis calculation.

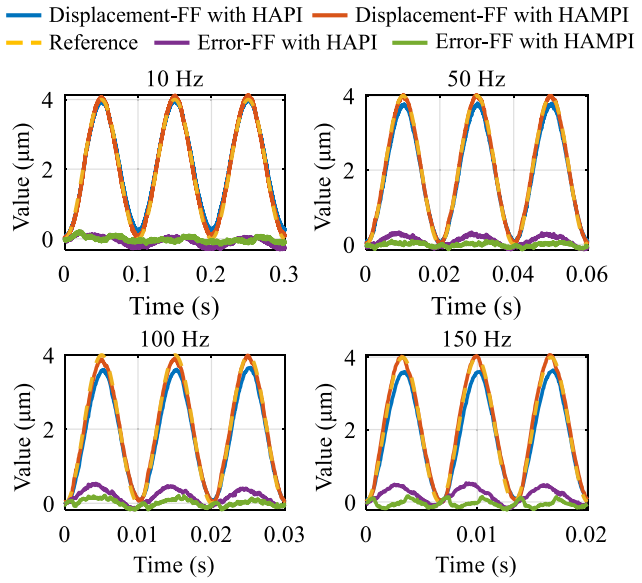

Fig. 15. Position tracking results of the feedforward controller with HAPI and HAMPI in different input rates.

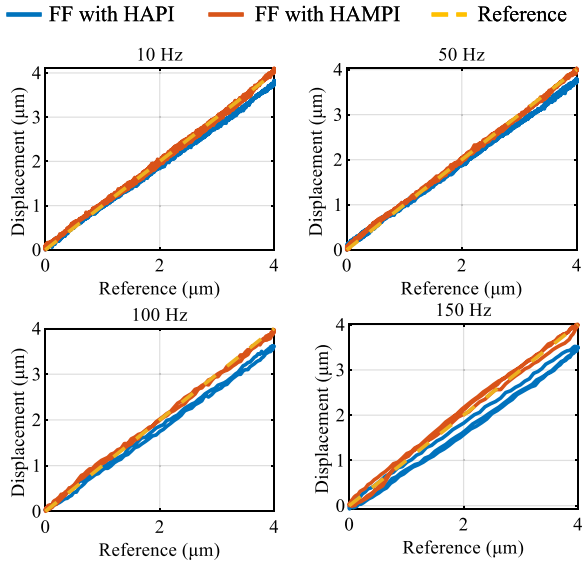

Fig. 16. Compensation results of the feedforward controller with HAPI and HAMPI in different input rates.

5. Experimental evaluation

5.1. Experimental platform

An experimental platform was built to test the open-loop performance of the PEA, as shown in Fig. 10. The input voltage signal is generated by the RT-links real-time platform (Beijing Lingsi Chuangqi Technology Co., LTD, Links-Box-03), and linearly amplified by the power amplifier (AETechron Inc, 7224) into a voltage signal to directly excite the PEA. A capacitive displacement sensor (Harbin Core Tomorrow Technology Co., Ltd, E09. Cap) was employed to measure the output displacement of PEA. The signals from the displacement sensor and the controller are collected and stored by the RT-links real-time platform. The open-loop displacement test experiment is conducted on an optical platform (Beijing keying Chuangtuo Technology Development Co., Ltd, LY102GP900X900X800H) to isolate external vibrations and minimize their interference with the test results.

The experimental methodology is as follows. Because the piezoelectric ceramics cannot withstand the negative voltage, the excitation signal is a sinusoidal signal with a DC bias. The amplitude of the DC bias is equal to the amplitude of the sinusoidal signal. In detail, the open-loop test experiment uses two types of input signals: (1) A step signal with an amplitude of 10 V. (2) Sinusoidal signals with different amplitudes, DC biases, and frequencies. During the experiment, these two signals are input into the piezoelectric actuator, and the displacement of the actuator is tested under different signal conditions. As to the feedforward control test, the reference signal also has a DC bias to avoid negative voltage.

5.2. The validation of HAMPI model

The employment of the HAMPI model allows the PEA's model to take into account the dynamic hysteresis including expansion and rotation. To validate the HAMPI model, this section compares the HAPI model, the rate-dependent PI (RDPI) model in [27] and the HAMPI model's output with the experimental hysteresis loops under different input rates (50–500 Hz) and different amplitude of 50, 100 and 140 V.

As shown in Fig. 11, the reference data consists of experimental hysteresis loops obtained under different input rates (50–500 Hz) with an excitation amplitude of 50 V. Compared to the HAPI model and RDPI model, the HAMPI model provides results that are highly consistent with the experimental data when the operating frequencies range from 100 to 500 Hz. To further assess the HAMPI model's ability to describe hysteresis loops under varying excitation amplitudes, excitation amplitudes of 100 V and 50 V are also considered. The corresponding model validation results are presented in Figs. 12 and 13. The findings demonstrate that, compared to the HAPI model and RDPI model, the HAMPI model proposed in this study more accurately describes hysteresis loops across different excitation amplitudes and frequencies. Additionally,

Table 4
RMSE (NRMSE) for HAPI, RDPI and HAMPI under 140 V excitation.

Freq. (Hz)	HAPI	RDPI	HAMPI
50	0.58 (3.83%)	0.22 (1.47%)	0.32 (2.10%)
100	0.55 (3.68%)	0.48 (3.18%)	0.24 (1.60%)
200	0.69 (4.71%)	0.70 (4.75%)	0.19 (1.26%)
300	0.69 (4.70%)	0.92 (6.26%)	0.21 (1.40%)
400	0.78 (5.22%)	1.21 (8.18%)	0.32 (2.14%)
500	0.85 (5.58%)	1.60 (10.44%)	0.47 (3.07%)

Table 5
RMSE (NRMSE) for controllers with HAPI and HAMPI.

Freq. (Hz)	HAPI	HAMPI
10	0.16 (3.92%)	0.06 (1.50%)
50	0.15 (3.86%)	0.05 (1.28%)
100	0.25 (6.71%)	0.06 (1.61%)
150	0.35 (8.75%)	0.09 (2.25%)

the HAMPI model simultaneously captures the rate-dependent rotation and expansion of the hysteresis loops with greater precision.

To quantify modeling errors of HAPI, RDPI and HAMPI model under different input rates (50–500 Hz) with the excitation amplitude of 140 V, the root-mean-square error (RMSE) and the relative root-mean-square error (NRMSE) are calculated in this paper. They are defined as follows:

$$\mathrm{RMSE} = \sqrt{1/T \int_0^T \left|x(t) - x_d(t)\right|^2 dt} \tag{25}$$

$$\mathrm{NRMSE} = \frac{\mathrm{RMSE}}{\max(x(t)) - \min(x(t))} \times 100\%, \tag{26}$$

where $x(t)$ and $x_d(t)$ are the simulated and measured displacements respectively, and T is the total time. The calculation results are shown in Table 4 and Fig. 14.

5.3. Experiment of the feedforward controller with HAMPI model

The feedforward control experiments compare the feedforward controller with HAMPI and HAPI models, both using the same linear dynamics compensation $\hat{G}^{-1}(\cdot)$. Hence, the controller performance merely depends on the accuracy of the hysteresis models. Since the sampling rate is limited to 50 kHz due to limitations in the control system hardware, the tracking reference is set as a 4 μm sinusoidal reference signal at 10–150 Hz.

The results are shown in Figs. 15 and 16. It is obvious that the HAMPI-based feedforward controller performs better position tracking and hysteresis compensation under 10–150 Hz, which further validates the effectiveness of the proposed model. The displacement attenuation issue in HAPI-based feedforward control caused by the rotation of hysteresis loops is also successfully addressed by the HAMPI model. The RMSE (NRMSE) of the two controllers are calculated as Table 5 shows.

6. Conclusion

This paper proposes a Hammerstein-like architecture with a modified Prandtl–Ishlinskii (HAMPI) model to accurately model the expansion and rotation of hysteresis loops. The model uses dynamic weights that directly account for these phenomena. A HAMPI-based feedforward controller is designed to cancel dynamic hysteresis using the approximate inverse of linear dynamics and an inverse multiplicative structure. Simulation and experimental results show that:

(1) The HAMPI model more accurately captures dynamic hysteresis, including expansion and rotation, at higher rates (50–500 Hz), with RMSE (resp. NRMSE) less than 0.47 μm (resp. 3.07%) compared to the HAPI model and the RDPI model.

(2) The HAMPI-based controller achieves better hysteresis cancellation than the HAPI-based one below 150 Hz with RMSE (resp. NRMSE) under 0.09 μm (resp. 2.25%). It addresses displacement attenuation issues caused by the rotation of hysteresis loops.

Overall, the HAMPI model offers high accuracy in modeling dynamic hysteresis and shows strong potential for high-rate PEA applications in both modeling and control.

CRediT authorship contribution statement

Yunzhi Zhang: Writing – original draft, Visualization, Validation, Methodology, Investigation, Formal analysis, Data curation, Conceptualization. **Jie Ling:** Writing – review & editing, Supervision, Funding acquisition. **Micky Rakotondrabe:** Writing – review & editing, Supervision, Project administration. **Yuchuan Zhu:** Supervision, Resources, Project administration. **Dan Wang:** Supervision, Resources, Investigation.

Declaration of competing interest

The authors declare that they have no known competing financial interests or personal relationships that could have appeared to influence the work reported in this paper.

Acknowledgments

This work was supported by International Joint Laboratory of Sustainable Manufacturing, Ministry of Education, the Fundamental Research Funds for the Central Universities, China, No. NG2024016 and the Aeronautical Science Foundation of China, No. 20220007052001.

Appendix. Abbreviations

- **PEA:** Piezoelectric actuator.
- **PI model:** Prandtl–Ishlinskii model.
- **HAMPI:** Hammerstein architecture with modified rate-dependent Prandtl–Ishlinskii model.
- **HAPI:** Hammerstein architecture with the Prandtl–Ishlinskii model.
- **ZPETC:** Zero-phase-error tracking control.
- **ZMETC:** Zero-magnitude-error tracking control.
- **NPZ-Ignore:** Nonminimum-phase zeros ignore.
- **RDPI:** Rate-dependent Prandtl–Ishlinskii model.
- **RMSE:** Root-mean-square error.
- **NRMSE:** Relative root-mean-square error.

Data availability

Data will be made available on request.

References

[1] Ling J, Chen L, Feng Z, Zhu Y. Development and test of a high speed pusher-type inchworm piezoelectric actuator with asymmetric driving and clamping configuration. Mech Mach Theory 2022;176:104997.
[2] An D, Li J, Yang Y, Xu Y, Shao M, Li Y. Compensation method for complex hysteresis characteristics on piezoelectric actuator based on separated level-loop Prandtl–Ishlinskii model. Nonlinear Dynam 2022;1–19.
[3] Zhang Y, Ling J, Zhu Y. Development and fault-tolerant control of a distributed piezoelectric stack actuator. Smart Mater Struct 2024;33(9):095003.
[4] Hassani V, Tjahjowidodo T, Do TN. A survey on hysteresis modeling, identification and control. Mech Syst Signal Process 2014;49(1–2):209–33.
[5] Yang M, Li C, Gu G, Zhu L. A rate-dependent Prandtl-Ishlinskii model for piezoelectric actuators using the dynamic envelope function based play operator. Front Mech Eng 2015;10(1):37–42.
[6] Wang Y, Yu Y, Shen C, Zhou M. Precise motion tracking of piezo-actuated stages via a neural network-based data-driven adaptive predictive controller. Nonlinear Dynam 2023;111(20):19047–72.

[7] Ling J, Feng Z, Zheng D, Yang J, Yu H, Xiao X. Robust adaptive motion tracking of piezoelectric actuated stages using online neural-network-based sliding mode control. Mech Syst Signal Process 2021;150:107235.
[8] Ming M, Ling J, Feng Z, Xiao X. A model prediction control design for inverse multiplicative structure based feedforward hysteresis compensation of a piezo nanopositioning stage. Int J Precis Eng Manuf 2018;19(11):1699–708.
[9] Ling J, Feng Z, Chen L, Zhu Y, Pan Y. Neural network-based iterative learning control of a piezo-driven nanopositioning stage. Precis Eng 2023;81:112–23.
[10] Feng Z, Ming M, Ling J, Xiao X, Yang Z-X, Wan F. Fractional delay filter based repetitive control for precision tracking: Design and application to a piezoelectric nanopositioning stage. Mech Syst Signal Process 2022;164:108249.
[11] Rakotondrabe M. Bouc–Wen modeling and inverse multiplicative structure to compensate hysteresis nonlinearity in piezoelectric actuators. IEEE Trans Autom Sci Eng 2010;8(2):428–31.
[12] Hong GS, San Wong Y, et al. Integral sliding mode control for fast tool servo diamond turning of micro-structured surfaces. Int J Autom Technol 2011;5(1):4–10.
[13] Aguirre G, Janssens T, Van Brussel H, Al-Bender F. Asymmetric-hysteresis compensation in piezoelectric actuators. Mech Syst Signal Process 2012;30:218–31.
[14] Al Janaideh M, Rakheja S, Su C-Y. Experimental characterization and modeling of rate-dependent hysteresis of a piezoceramic actuator. Mechatronics 2009;19(5):656–70.
[15] Al Janaideh M, Krejčí P. A rheological model for the rate-dependent Prandtl-Ishlinskii model. In: 52nd IEEE conference on decision and control. IEEE; 2013, p. 6646–51.
[16] Alatawneh N, Al Janaideh M. A frequency-dependent Prandtl–Ishlinskii model of hysteresis loop under rotating magnetic fields. IEEE Trans Power Deliv 2019;34(6):2263–5.
[17] Nie L, Luo Y, Gao W, Zhou M. Rate-dependent asymmetric hysteresis modeling and robust adaptive trajectory tracking for piezoelectric micropositioning stages. Nonlinear Dynam 2022;108(3):2023–43.
[18] Yang M, Li C, Gu G, Zhu L. Modeling and compensating the dynamic hysteresis of piezoelectric actuators via a modified rate-dependent Prandtl–Ishlinskii model. Smart Mater Struct 2015;24(12):125006.
[19] Gu G, Li C, Zhu L, Su C. Modeling and identification of piezoelectric-actuated stages cascading hysteresis nonlinearity with linear dynamics. IEEE/ASME Trans Mechatronics 2015;21(3):1792–7.
[20] Li C, Li L, Gu G, Zhu L. Modeling of rate-dependent hysteresis in piezoelectric actuators using a Hammerstein-like structure with a modified Bouc-Wen model. In: Intelligent robotics and applications: 9th international conference. Springer; 2016, p. 672–84.
[21] Zhang M, Cui X, Xiu Q, Zhuang J, Yang X. Dynamic modeling and controlling of piezoelectric actuator using a modified preisach operator based Hammerstein model. Int J Precis Eng Manuf 2023;24(4):537–46.
[22] Peng X, Guo Z, Wei X, Liu X. A rate-dependent hysteresis model for giant magnetostrictive actuators using the dynamic weight and dynamic threshold based modified Prandtl-Ishlinskii model. In: 2017 29th Chinese control and decision conference. IEEE; 2017, p. 1651–6.
[23] Al Janaideh M, Al Saaideh M, Tan X. The Prandtl–Ishlinskii hysteresis model: fundamentals of the model and its inverse compensator [lecture notes]. IEEE Control Syst Mag 2023;43(2):66–84.
[24] Butterworth JA, Pao LY, Abramovitch DY. The effect of nonminimum-phase zero locations on the performance of feedforward model-inverse control techniques in discrete-time systems. In: 2008 American control conference. IEEE; 2008, p. 2696–702.
[25] Torfs D, De Schutter J, Swevers J. Extended bandwidth zero phase error tracking control of nonminimal phase systems. J Dyn Syst Meas Control 1992;114(3):347–51.
[26] Rakotondrabe M. Classical Prandtl-Ishlinskii modeling and inverse multiplicative structure to compensate hysteresis in piezoactuators. In: 2012 American control conference. IEEE; 2012, p. 1646–51.
[27] Al Janaideh M, Krejčí P. Inverse rate-dependent Prandtl–Ishlinskii model for feedforward compensation of hysteresis in a piezomicropositioning actuator. IEEE/ASME Trans Mechatronics 2012;18(5):1498–507.